ARTICLE

Analytical Bond-order Potential for hcp-Y

Kai-min Fan[a,b], Li Yang[a*], Jing Tang[c], Qing-qiang Sun[a,d], Yun-ya Dai[a], Shu-ming Peng[e], Xiao-song Zhou[e], Xiao-tao Zu[a]

a. School of Physical Electronics, University of Electronic Science and Technology of China, Chengdu 610054, China
b. Department of Physics and Engineering Technology, Sichuan University of Arts and Science, Dazhou 635000, China
c. Department of Chemistry and Chemical Engineering, Sichuan University of Arts and Science, Dazhou 635000, China
d. School of Science, Huaihai Institute of Technology, Lianyungang 222005, China
e. Institute of Nuclear Physics and Chemistry, China Academy of Engineering Physics, Mianyang 621900, China

(Dated: Received on May 23, 2013; Accepted on August 16, 2013)

The lattice parameters, elastic constants, cohesive energy, structural energy differences, as well as the properties of point defects and planar defects of hexagonal close-packed yttrium (hcp-Y) have been studied with *ab initio* density functional theory for constructing an extensive database. Based on an analytical bond-order potential scheme, empirical many-body interatomic potential for hcp-Y has been developed. The model is fitted to some properties of Y, *e.g.*, the lattice parameters, elastic constants, bulk modulus, cohesive energy, vacancy formation energy, and the structural energy differences. The present potential has ability to reproduce defect properties including the self-interstitial atoms formation energies, vacancy formation energy, divacancy binding energy, as well as the bulk properties and the thermal dynamic properties.

Key words: Hexagonal close-packed yttrium, Bond-order potential, Density functional theory, Molecular dynamics

I. INTRODUCTION

Rare earth metals, including yttrium (Y), provide one of the most exciting areas for theoretical and experimental research due to their high capacity H storage [1]. In the last few years, properties of several hexagonal close-packed (hcp) metals have been reported using potential interactions, including yttrium (Y) [2, 3], erbium (Er) [3, 4], scandium (Sc) [2, 3], and dysprosium (Dy) [5]. Baskes and Johnson [3] have investigated Y-Y system using modified embedded atom method (MEAM) potential, which gives a realistic picture of structural energies for a number of hexagonal crystal lattices. However, the divacancy in Y is unbound because of its negative binding energy, moreover, the properties of self-interstitial atoms (SIAs) were not studied by their potential. Hu *et al.* have investigated several hcp metals, and proposed analytic modified embedded atom method (AMEAM) for Y [2]. This Y-Y AMEAM potential was fitted to lattice constants, elastic constants, cohesive energy, vacancy formation energy, and the structural energy differences [2]. Most of the crystal properties of Y, for example, mono-vacancy formation energies, surface energies, divacancy formation energies, and divacancy binding energies have been reproduced well by the AMEAM, but the structural energy difference is rather small, especially between fcc and hcp.

Brenner and co-workers have extended the Tersoff potential [6] to pure carbon and small hydrocarbon molecules systems by adequately considering reactive scheme [7, 8], and it was used to describe the ternary W-C-H system [9]. The bond-order potential of bcc tungsten (W) has been constructed, which is a semiempirical potential scheme [10]. There are also some reports on the studies of bond-order potentials (BOP) for hcp metals [4, 11, 12]. Recently, the analytical bond-order potentials scheme has been extended to Er-H, W-H and W-He systems [4, 13, 14]. In the present work, the Y-Y interaction potential is fitted using the BOP scheme.

The properties of some of point defects in Y can be found in experiment results, but most of them are very scarce, such as the properties of SIAs. Density functional theory calculations (DFTC) have been successfully used to study the point defects in metal crystals [15−19]. In our previous work, the properties of SIAs,

*Author to whom correspondence should be addressed. E-mail: yanglildk@uestc.edu.cn

TABLE I Number of k-points and supercell size in the present DFTC for cohesive energy (E_c), elastic constant (C_{ij}), lattice parameters (a and c), dimer, surface energies ($E^f_{\rm surf}$) and the point defect.

	Point defect	E_c	Dimer	C_{ij}	$E^f_{\rm surf}$	a and c
Supercell size	4×4×3	4×4×3	15 Å×15 Å×15 Å	1×1×1	2×2(atoms)×9(layers)	1×1×1
k-points	2×2×2	2×2×2	1×1×1	11×11×9	9×9×1	11×11×9

vacancies, and single H and He atoms in hcp Er and Sc were studied by DFTC [15, 16]. In the present work, the DFTC are performed to obtain as many properties as possible for the parameterization of the Y-Y interaction potential. Using the available experimental data and the DFTC results, we have constructed an analytical BOP to model the properties of hcp-Y, which well reproduces many properties of hcp-Y, such as self-interstitial defect formation energies, structural properties, melting point, and relevant bulk properties.

II. COMPUTATIONAL METHOD

A. Potential formalism

The analytic potential form used for the Y-Y atomic potential was derived from the Brenner potential [7] and it is essentially the same as that of the Tersoff potential [6], which takes into account the chemical environment of the atoms as well as their geometrical relationships to one another. The detailed descriptions of the BOP formalism were demonstrated in Refs.[20−23]. The analytical BOP is summarized briefly in this work. The total potential energy is written as a sum over individual bond energies.

$$E=\sum_{i>j} f^{\rm c}_{ij}(r_{ij})\left[V^{\rm R}_{ij}-\frac{b_{ij}+b_{ji}}{2}V^{\rm A}_{ij}(r_{ij})\right] \quad (1)$$

$$V^{\rm R}(r)=\frac{D_0}{S-1}\exp[-\beta\sqrt{2S}(r-r_0)] \quad (2)$$

$$V^{\rm A}(r)=\frac{SD_0}{S-1}\exp[-\beta\sqrt{2/S}(r-r_0)] \quad (3)$$

where E is the expression of total potential energy, $V^{\rm R}(r)$ and $V^{\rm A}(r)$ are the pairwise repulsive and attractive contributions, D_0 and r_0 represent the bond energy and bond length of a dimer. In these above equations, D_0, r_0, S, and β are all adjustable parameters. The cut-off function $f^{\rm c}(r)$, bond-order parameter b_{ij}, and the angular function $g(\theta)$ are described by the following equations:

$$f^{\rm c}(r)=\begin{cases}1, & r\le R-D\\ \dfrac{1}{2}-\dfrac{1}{2}\sin\left(\dfrac{\pi}{2}\dfrac{r-R}{D}\right), & |R-r|\le D\\ 0, & r\ge R+D\end{cases} \quad (4)$$

$$b_{ij}=(1+\chi_{ij})^{-1/2} \quad (5)$$

$$g(\theta)=\gamma\left(1+\frac{c^2}{d^2}-\frac{c^2}{d^2+h+\cos\theta}\right) \quad (6)$$

$$\chi_{ij}=\sum_{k\neq i,j} f^{\rm c}_{ik}(r_{ik})g_{ik}(\theta_{ijk})\exp[\alpha_{ijk}(r_{ij}-r_{ik})] \quad (7)$$

where D, R, c, d, γ, h, and α_{ijk} are adjustable parameters.

B. Methodology of fitting

A substantial fitting database must be constructed after the potential formulism was determined. Some available experimental data of the lattice constants, elastic constants, cohesive energy and bulk moduli of Y can be found.

The DFTC are performed to complement the database by using the VASP (Vienna *ab initio* Simulation Package) code [24]. The interactions between ions and electrons are described using the projector-augmented wave (PAW) method [25, 26], and the exchange and correlation functions by the generalized gradient approximation (GGA) of Perdew and Wang (PW91) [27]. The pseudopotential of Y is taken from the VASP library. The relaxations of the atomic positions and the optimizations of the shape and size of the supercell are performed using the plane-wave basis sets with an energy cutoff of 300 eV. Once the relaxation is completed, the total-energy of the systems is accurately determined using the tetrahedron method with Blöchl corrections. The cohesive energy, elastic constant, lattice parameters, surface energies, the properties of point defects and dimer have been investigated by the DFTC. In the DFTC, supercells scaled from the 2-atom cell are chosen, Gamma-centered grids are used in the all calculations, and the number of k-points, supercell size and the properties carried out in this work are listed in Table I. As shown in Table I, to model the metal surface, a slab with 9 layers (2×2 atoms per layer) is employed, which is separated by a 15-Å vacuum region.

The fitting database includes the lattice parameters, cohesive energy, bulk modulus, elastic constants, structural energy differences and the vacancy formation energy for Y, which are from experimental and our DFTC data. In order to obtain a high-quality potential, a set of suitable potential parameters are required which can reproduce energetics and structural properties of hcp-Y. Starting with a set of initial guess values, these param-

DOI:10.1063/1674-0068/26/05/526-532

TABLE II Formation energies (in eV) for the SIAs of several possible configurations in hcp-Y for a 96-atom supercell.

k-points	O	S	C	T	BO	BS	BC	BT
4×4×4	2.44	2.85	2.73	2.86	2.07	2.54	2.07	3.16
2×2×2	2.48	2.86	2.76	2.90	2.12	2.61	2.12	3.19

eters of potential are optimized by adjusting the properties calculated by the potential to fit these calculated and experimental data from the fitting database. Once a set of parameters is found, the properties which are not the data of the fitting database will be tested by the potential, for example, the divacancy binding energies, self-interstitial defects formation energies, melting point and the surface energies of Y. If the parameters do not perform adequately, a new set of parameters must be searched until the potential parameters are satisfying.

U is the objective function, which determines if each set of fitting parameters can be accepted, defined as [4, 14]

$$U = \sum_i w_i [f_i(\lambda^n) - F_i]^2 \tag{8}$$

The structure properties and the defect formation energies are obtained by using the MD code LAMMPS [28, 29]. A $5a\times4\sqrt{3}a\times4c$ cubic box with 320 Y atoms is used in the fitting procedure for the hcp-Y, where a and c are the lattice parameters [4]. The potential parameters calculated for the Y-Y interactions are compiled as follows, D_0=2.64686 eV, R_0=2.99839 Å, β=0.79884 Å^{-1}, S=3.34600, γ=0.05577, c=1.34719, d=0.34880, h=−0.49445, R=5.74046 Å, and D=0.22582 Å.

III. RESULTS AND DISCUSSION

A. Data of DFTC

In the present DFTC, a 96-atom supercell is used to calculate the point defect properties in hcp-Y, and the results are shown in Table II. For testing the effect of k-points on the calculated results, 2×2×2 k-points and 4×4×4 k-points are considered. The definitions of configurations for SIAs in hcp structure crystal are used extensively elsewhere [2, 4, 23], the initial configurations of SIAs for hcp-Y are illustrated in Fig.1. As shown in Fig.1, T is tetrahedral interstice, O represents octahedral interstice, the C site (crowdion) is midway between two nearest-neighbor atoms in the non-basal plane, and S represents the position of one atom in a ⟨0001⟩ split dumb-bell configuration. BT and BO represent the corresponding projected positions of T and O sites in the basal plane. BC site is a crowdion midway between two nearest neighbors in the basal plane and the configuration of BS is a split (dumbbell) in the basal plane.

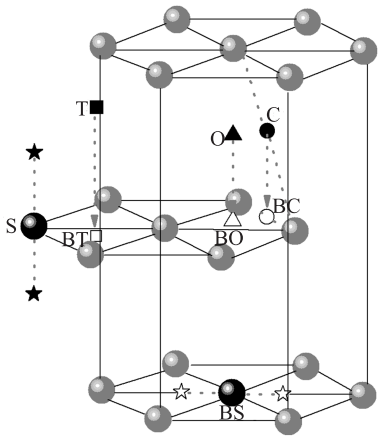

FIG. 1 Self-interstitial configurations in hcp lattice. T stands for tetrahedral, O is octahedral, C is crowdion, S represents split dumbbell, and BT, BO, BC, and BS are the corresponding basal plane positions. The gray spheres are the hcp lattice sites, and the black spheres represent the vacant lattice sites in the S and BS configurations. For interpretation of the color in this figure legend, the reader can refer to the web version of this article.

The SIAs formation energies are defined by [15, 23]

$$E_i^f = E_{N+1} - (N+1)E_{\rm coh} \tag{9}$$

where E_{N+1} is the total energy of a computational supercell with one self-interstitial Y atoms, N represents the number of atoms in the supercell without self-interstitial atom, and $E_{\rm coh}$ is the energy per Y atom in a perfect hcp Y crystal.

From Table II, one can see that the formation energies of the SIAs depend slightly on the numbers of k-points used. The largest difference of the formation energies for the SIAs due to using different k-points is less than 2.7%. Moreover, it can be seen that the relative stability of the SIAs is not affected by the k-points used. For the calculations with 2×2×2 k-points and 4×4×4 k-points, the most stable configuration of the SIAs is BO site, the BT interstitial has the highest formation energies among the seven configurations considered, which are similar to those in hcp-Er. In our previous studies, the most stable and unstable self-interstitial configurations are also BO and BT in hcp-Er [4, 15]. In addition, the DFTC gave the BO to be the most stable in hcp-Sc [16], in contrast to those in hcp-Zr where two or more configurations may coexist [30]. The lattice parameters, elastic constants, bulk modulus, cohesive energy, vacancy formation energy, structural energy differences, divacancy binding energies, surface energies, and the properties of Y-Y dimer are also studied by DFTC, those data are listed in Tables III and IV, which will be discussed and compared with the results of the present BOP in section B and C.

DOI:10.1063/1674-0068/26/05/526-532

TABLE III Fitted physical properties of hcp-Y obtained by the present BOP, and those from the DFTC, experiments (Exp.) and other potentials, the cohesive energy (E_c) and structural energy differences (ΔE) are in eV/atom, the elastic constants (C_{ij}) is in GPa, the relaxed vacancy formation energy ($E^f_{\rm vac}$) and dimer bond energy ($E_{\rm dimer}$) are in eV.

	BOP	Exp.	DFTC	(A)MEAM		BOP	Exp.	DFTC	(A)MEAM
E_c	4.36	4.37 [34]	4.31		B/GPa	41.5	41.3 [31]	41.6	41.5 [3]
a	3.647	3.647 [33]	3.637	3.637 [3]	$\Delta E_{\rm hcp\to bcc}$	0.112		0.127	0.044 [2], 0.300 [3]
c	5.730	5.731 [33]	5.674	5.701 [3]	$\Delta E_{\rm hcp\to fcc}$	0.016		0.022	0.002 [2], 0.052 [3]
C_{11}	75.9	77.9 [31]	76.9	86.7 [3]	$\Delta E_{\rm hcp\to sc}$	0.692		0.772	0.680 [3]
C_{12}	27.2	29.3 [31]	24.6	31.6 [3]	$\Delta E_{\rm hcp\to dia}$	1.629		1.939	2.050 [3]
C_{13}	22.9	20.1 [31]	22.9	17.5 [3]	$E^f_{\rm vac}$	1.28	1.25 [32]	1.69	1.22 [2], 1.25 [3]
C_{33}	75.5	77.0 [31]	79.6	67.1 [3]	$E_{\rm dimer}$	2.65		1.84	
C_{44}	22.6	24.3 [31]	25.5	24.4 [3]	r_0	3.00		2.92	

TABLE IV Calculated physical properties of hcp-Y using the present BOP, and those from the present DFTC, experiments (Exp.) and other potentials. The properties include the divacancy binding energy $E_{\rm b}$ (in eV), self-interstitial formation energy E^f_i (in eV), monovacancy formation volume V^f_v (in Ω_0), divacancy formation volume $V^f_{\rm div}$ (in Ω_0), self-interstitial formation volume V^f_i (in Ω_0), the surface energies $E^f_{\rm surf}$ (J/m^2) and melting point T_m (in K) of hcp-Y.

	Config.	BOP	Exp.	DFTC	(A)MEAM		Config.	BOP	Exp.	DFTC	(A)MEAM
$E_{\rm b}$	In	0.337		0.119	0.15 [2], −0.06 [3]	V^f_i	T	1.059			0.85 [2]
	Out	0.329		0.116	0.12 [2], −0.03 [3]		O	1.027			1.04 [2]
E^f_i	T	3.04		2.90	3.23 [2]		C	0.899			0.97 [2]
	O	2.93		2.48	3.32 [2]		S	0.931			0.98 [2]
	C	2.95		2.76	3.28 [2]		BO	0.835			0.92 [2]
	S	3.07		2.86	3.28 [2]		BS	0.963			0.88 [2]
	BO	2.69		2.12	3.36 [2]		BC	0.867			0.85 [2]
	BS	2.91		2.61	3.23 [2]		BT	0.963			0.88 [2]
	BC	2.69		2.12	3.23 [2]	$E^f_{\rm surf}$	Basal	0.684	1.125 [32]	0.991	0.623 [2], 1.001 [3]
	BT	2.96		3.19	3.23 [2]		Prism	0.678	1.125 [32]	1.160	0.626 [2], 0.738 [3]
V^f_v		0.712			0.93 [2]	T_m		1575±25	1799 [38]		
$V^f_{\rm div}$	In	1.392			1.86 [2]						
	Out	1.392			1.86 [2]						

B. Fitted properties

The lattice parameters, cohesive energy, elastic constants, vacancy formation energy, bulk modulus, and the structural energy differences are used in the fitting process. The present BOP calculations are all performed with a $10a\times6\sqrt{3}a\times6$c cubic box expect the calculations of melting point, and this box contains 1440 Y atoms. Table III shows the results of the present model, and those corresponding data from the experiments, other interatomic potentials and the present DFTC for comparison.

It is clear that E_c calculated by the BOP is 4.36 eV/atom, which agrees well with the experimental value (4.37 eV/atom) and the value from the present DFTC (4.31 eV/atom). The lattice parameters given by the present BOP are almost the same as the experiment results and close to the data of DFTC. Moreover, the bulk modulus is well reproduced by the present BOP. Baskes and Johnson investigated hcp-Y using the MEAM scheme, in which the bulk modulus with angular dependence agrees with experimental results [31]. Nevertheless, the differences between their results and the experimental values of elastic constants [31] are significant, especially for C_{11}, C_{13}, and C_{33}. The largest difference is up to 23.58%. From Table IV, it can also be found that the five independent elastic constants calculated by the present BOP almost agree with our DFTC. The differences in the elastic constants between the present BOP and the DFTC is less than 11.4%, while the largest difference in the elastic constants between the present BOP calculations and the results from experiments is about 13.9%.

The lattice stability of other structures, including bcc, fcc, simple cubic (sc) and diamond cubic (dia), relative to the hcp structure is predicted. We did not find available experimental data of the structural energy difference of Y. In the present work, we have calculated the structural energy differences ($\Delta E_{\rm hcp\to bcc}$, $\Delta E_{\rm hcp\to fcc}$, $\Delta E_{\rm hcp\to sc}$, $\Delta E_{\rm hcp\to dia}$) by DFTC, which

DOI:10.1063/1674-0068/26/05/526-532

have been performed to fit the present BOP parameters. The structural energy differences calculated by the present BOP and DFTC are included in Table III together with the data from other potential models [2, 3]. The present DFTC displays that the four structural energy differences are all positive as shown in Table III, and it implies that the hcp lattice fitted by the present BOP is the most stable structure. It should be noted that the energy differences are well reproduced by the present BOP, compared to the data from the other two potential models, as listed in Table III. One can find that Baskes's model gives large structural energy differences for bcc and fcc, while Hu's model predicted a rather small structural energy difference for the two structures.

In experiment, all the properties of point defect of hcp-Y are scarce except the vacancy formation energy. It is necessary to fit the properties of vacancy in the fitting process. The vacancy formation energies are calculated according to the following equation:

$$E^f_{V_m} = E_{V_m} - (N-m)E_{\rm coh} \tag{10}$$

E_{V_m} represents the total energy of a supercell with vacancies, m is the number of vacancies, N is the number of atoms of the perfect hcp supercell, $E_{\rm coh}$ is the energy per Y atom in a perfect hcp Y crystal.

It is evident that in the present BOP the monovacancy formation energy is calculated to be 1.28 eV, which agrees with the experimental value of 1.25 eV [32]. However, the vacancy formation energy is determined to be 1.69 eV by the DFTC, and it is significantly higher than the present BOP data and the experiment result, which may be due to the overestimation of the vacancy formation energy by the DFTC [4].

Among the properties considered in this work, $E_{\rm dimer}$ and r_0 are adjustable parameters in the present BOP (see Eq.(3)), but they are assigned relatively low weights in the fitting procedure. It is obvious that the dimer bond energy with the value of 2.65 eV is only roughly conformably with the present DFTC value of 1.84 eV, while the value of bond distance is estimated to be 3.00 Å, which is in good agreement with the result of DFTC as shown in Table III.

C. Tests of the potential

To make sure if the present potential is reliable, additional physical properties, such as the formation energies of SIAs, divacancy binding energy, surface energies and melting point have been tested. A simulation box containing 1008 Y atoms is used to test the melting point. These results from the present BOP, DFTC, experiments and other potential models are summarized in Table IV.

The properties of divacancy have been investigated by the present BOP. The divacancy binding energy is defined by

$$E_{\rm b} = 2E^f_{\rm s} - E^f_{\rm di} \tag{11}$$

$E^f_{\rm s}$ is the formation energy of a single vacancy, $E^f_{\rm di}$ represents the divacancy formation energy [4, 23]. In Table IV, the divacancy binding energy E_b denoted with "In" is the binding energy of two near vacancies in the basal plane, while that labeled by "Out" represents two near vacancies in the non-basal plane. It is clearly found that divacancy binding energies given by the present BOP are positive, which is in agreement with previous studies on hcp metals [2, 4, 35] and agrees with our DFTC. This indicates that the divacancy configurations are stable, which is different from the results of the potential model constructed by Baskes and Johnson [3]. It can also be found that the E_b in the basal plane is somewhat higher than that in the non-basal plane, which implies the divacancy preferred to forming in the basal plane as other hcp metals (Er, Dy, Gd, Ho, Nd, Pr, and Tb) [2, 4, 5].

The formation energies of SIAs have been evaluated by the present BOP. It can be seen from Table IV, most of configurations, *e.g.*, T, O, C, S, BO, BS, and BT, are stable, while the BC site is unstable which transfers to site BO, which is similar to the properties of SIAs in hcp-Er [4]. The DFTC results indicate that BO site is the most stable configuration, followed by the O, BS and C sites, but the BC configuration is unstable and decays to BO. Compared to the DFTC, the present potential, although the formation energies of SIAs are larger than the DFTC results, gives the same ground state interstitial configuration, since the present simulations show the BO to be the most stable site with the lowest formation energy of 2.69 eV, and the present DFTC indicate that the formation energy of BO (2.12 eV) is also the lowest. Note that the formation energy of O site is lower than that of site T, which agrees well with the conclusions from the DFTC and other model [2]. The formation volumes of a monovacancy, divacancies and self-interstitial atoms have been calculated with the present BOP (see Table IV), which are almost conformable with Hu's results [2]. Thus, the present BOP is able to predict the properties of point defects.

The surface energies have been calculated and the corresponding values are listed in Table IV. The surface energy is given by

$$E_{\rm surf} = \frac{E_{\rm slab} - E_{\rm perf}}{2A} \tag{12}$$

where $E_{\rm slab}$ is the total energy of a 36-atom slab, $E_{\rm perf}$ is the total energy of a perfect bulk crystal with 36 atoms, and A is the surface area.

As shown in Table IV, the surface energies of the basal and prism planes calculated by the present BOP are 0.684 and 0.678 J/m^2 in sequence, which are close

DOI:10.1063/1674-0068/26/05/526-532

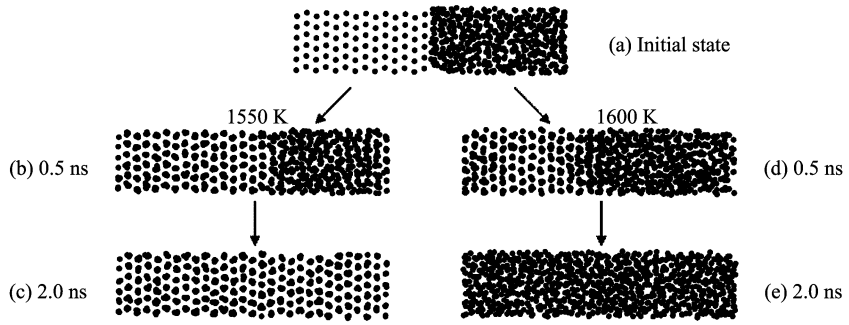

FIG. 2 Melting process of Y crystal. (a) Initial state of solid-liquid interface, (b) relaxed the initial state at 1550 K for 0.5 ns, (c) relaxed the initial state at 1550 K for 2.0 ns, (d) relaxed the initial state at 1600 K for 0.5 ns, and (e) relaxed the initial state at 1600 K for 2.0 ns.

to the results of Hu *et al.* [2]. Although they are somewhat lower than the experiments (average surface energy 1.125 J/m^2) and the DFTC, the present BOP can describe the planar defect properties to some degree.

The melting temperature of hcp-Y is tested by modelling a solid-liquid interface at zero pressure and different temperatures [4, 13, 36]. A 14×3×6 simulation box containing 1008 Y atoms has been employed to study the melting point of Y, where the temperature and pressure are controlled by the Berendsen thermostat and barostat [4, 37]. As shown in Fig.2, the simulation box is divided into two parts by the solid-liquid interface, one is fixed, another is relaxed at 3000 K for 5 ps, then the system are cooled and quenched to 0 K, which is the initial state of solid-liquid interface (see Fig.2(a)). The initially state is then relaxed at different temperatures, and equilibrated for time up to 2.0 ns. It can be seen from Fig.2(b), the crystalline phase begins to grow after relaxing 0.5 ns at 1550 K. However, Fig.2(d) shows that the left of the solid-liquid interface starts melting after relaxing 0.5 ns at 1600 K. The complete melting is observed after relaxing 2.0 ns at 1600 K, as shown in Fig.2(e), while when the system is relaxed at 1550 K, a stable hcp lattice grows in 2.0 ns, which is clearly demonstrated in Fig.2(c). Thus, an estimate of the melting point is given to be 1575±25 K, 224 K lower than experimental value (1799 K) [38]. It is difficult to well reproduce melting points by interatomic potential, *e.g.*, the melting point of W from MEAM is 4600 K [39], 910 K higher than the value from experiment, and Peng *et al.* calculated the melting point of Er to be 1350±50 K [4], which is 452 K lower than that of experimental value. The melting point may be connected with the formation energies of SIAs and vacancies [2, 35].

IV. CONCLUSION

We have presented calculations of the lattice parameters, elastic constants, cohesive energy, structural energy differences, as well as the properties of point defects, planar defects and dimer by using *ab initio* density functional theory for constructing an extensive database, then an analytical bond-order potential for Y has been developed. The present BOP provides good descriptions for the energetics and structural properties of hcp-Y, which well reproduces the elastic constants and bulk modulus. One point of interest is that the present potential gives that the divacancy configurations are stable. Especially, the present potential can reliably describe the structural stability, as well as the point defect properties of yttrium crystal. Furthermore, the fitted potential is able to reproduce the melting point of hcp-Y.

V. ACKNOWLEDGMENTS

This work was supported by the National Natural Science Foundation of China (No.10976007), the Natural Science Foundation of Sichuan Province Educational Bureau of China (No.11ZB141 and No.12ZB312), and the Natural Science Foundation of Sichuan University of Arts and Science (No.2012Z008Y).

[1] O. Blaschko, J. Pleschiutschning, L. Pintschovius, J. P. Burger, J. N. Daou, and P. Vajda, Phys. Rev. B **40**, 907 (1989).
[2] W. Y. Hu, B. W. Zhang, B. Y. Huang, F. Gao, and D. J. Bacon, Phys.: Condens. Matter **13**, 1193 (2001).
[3] M. I. Baskes and R. A. Johnson, Modelling Simul. Mater. Sci. Eng. **2**, 147 (1994).
[4] S. M. Peng, L. Yang, X. G. Long, H. H. Shen, Q. Q. Sun, X. T. Zu, and F. Gao, J. Phys. Chem. C **115**, 25097 (2011).
[5] W. Y. Hu, H. Q. Deng, X. J. Yuan, and M. Fukumoto, Eur. Phys. J. B **34**, 429 (2003).
[6] J. Tersoff, Phys. Rev. Lett **61**, 2879 (1988).
[7] D. W. Brenner, Phys. Rev. B **42**, 9458 (1990).
[8] D. W. Brenner, O. A. Shenderova, J. A. Harrison, J. A. Harrison, S. J. Stuart, B. Ni, and S. B. Sinnott, J. Phys.: Condens. Matter **14**, 783 (2002).

DOI:10.1063/1674-0068/26/05/526-532

[9] N. Juslin, P. Erhart, P. Träskelin, J. Nord, K. O. E. Henriksson, K. Nordlund, E. Salonen, and K. Albe, J. Appl. Phys **98**, 123520 (2005).
[10] M. Mrovec, R. Gröger, A. G. Bailey, D. Nguyen-Manh, C. Elsässer, and V. Vitek, Phys. Rev. B **75**, 104119 (2007).
[11] A. Girshick, A. M. Bratkovsky, D. G. Pettifort, and V. Vitek, Philosophical Magazine A **77**, 981 (1998).
[12] R. Drautz and D. G. Pettifor, Phys. Rev. B **74**, 174117 (2006).
[13] X. C. Li, X. L. Shu, Y. N. Liu, F. Gao, and G. H. Lu, J. Nucl. Mater **408**, 12 (2011).
[14] X. C. Li, X. L. Shu, Y. N. Liu, Y. Yu, F. Gao, and G. H. Lu, J. Nucl. Mater **426**, 31 (2012).
[15] L. Yang, S. M. Peng, X. G. Long, F. Gao, H. L. Heinisch, R. J. Kurtz, and X. T. Zu, J. Appl. Phys **107**, 054903 (2010).
[16] L. Yang, S. M. Peng, X. G. Long, F. Gao, H. L. Heinisch, R. J. Kurtz, and X. T. Zu, J. Phys.: Condens. Matter **23**, 035701 (2011).
[17] L. Chen, Y. L. Liu, H. B. Zhou, S. Jin, Y. Zhang, and G. H. Lu, Sci. China-Phys. Mech. Astron. **55**, 614 (2012).
[18] Y. L. Liu, Y. Zhang, H. B. Zhou, and G. H. Lu, Phys. Rev. B **79**, 172103 (2009).
[19] Y. L. Liu, H. B. Zhou, S. Jin, Y. Zhang, and G. H. Lu, J. Phys.: Condens. Matter **22**, 445504 (2010).
[20] P. Erhart and K. Albe, Phys. Rev. B **71**, 035211 (2005).
[21] K. Albe, K. Nordlund, J. Nord, and A. Kuronen, Phys. Rev. B **66**, 035205 (2002).
[22] F. Gao and W. Weber, J. Nucl. Instr. Meth. B **191**, 504 (2002).
[23] C. Björkas, N. Juslin, H. Timko, K. Vörtler, K. Nordlund, K. Henriksson, and P. Erhart, J. Phys.: Condens. Matter **21**, 445002 (2009).
[24] G. Kresse and J. Hafner, J. Phys.: Condens. Matter **6**, 8245 (1994).
[25] G. Kresse and D. Joubert, Phys. Rev. B **59**, 1758 (1999).
[26] P. E. Blöchl, Phys. Rev. B **50**, 17953 (1994).
[27] J. P. Perdew, J. A. Chevary, S. H. Vosko, K. A. Jackson, M. R. Pederson, D. J. Singh, and C. Fiolhais, Phys. Rev. B **46**, 6671 (1992).
[28] LAMMPS Molecular Dynamics Simulator, http://lammps.sandia.gov/
[29] S. Plimpton, J. Comp. Phys. **117**, 1 (1995).
[30] F. Willaime, J. Nucl. Mater **323**, 205 (2003).
[31] E. A. Brandes, *Smithells Metals Reference Book*, 6th Edn., London: Butterworths, 5 (1983).
[32] F. R. de Boer, R. Boom, W. C. M. Mattens, A. R. Miedema, and A. K. Niessen, *Cohesion in Metals Transition Metal Alloys*, Amsterdam: North-Holland, (1988).
[33] C. S. Barrett and T. B. Massalski, *Structure of Metals*, 3rd Edn, Oxford: Pergamon, 626 (1980).
[34] C. Kittel, *Introduction to Solid State Physics*, New York: Wiley, 74 (1976)
[35] D. J. Bacon, J. Nud. Mater **159**, 176 (1988).
[36] J. R. Morris, C. Z. Wang, K. M. Ho, and C. T. Chan, Phys. Rev. B **49**, 3109 (1994).
[37] K. Balasubramanian and Z. Ma, J. Phys. Chem. **95**, 9794 (1991).
[38] J. S. Wang, W. Liu, Y. Q. Liu, and M. L. Zhou, Appl. Surf. Sci. **251**, 89 (2005).
[39] B. J. Lee, M. I. Baskes, H. Kim, and Y. K. Cho, Phys. Rev. B **64**, 18410 (2001).

DOI:10.1063/1674-0068/26/05/526-532